Journal of Hazardous Materials 178 (2010) 729–738

Contents lists available at ScienceDirect

Journal of Hazardous Materials

journal homepage: www.elsevier.com/locate/jhazmat

Adsorption equilibrium of sulfur hexafluoride on multi-walled carbon nanotubes

Yu-Chun Chiang*, Po-Yun Wu

Department of Mechanical Engineering and Yuan Ze Fuel Cell Center, Yuan Ze University, 135 Yuan-Tung Rd., Chung-Li, Taoyuan 32003, Taiwan

ARTICLE INFO

Article history:
Received 7 October 2009
Received in revised form 16 January 2010
Accepted 1 February 2010
Available online 4 February 2010

Keywords:
Carbon nanotubes
Modification
Characterization
Sulfur hexafluoride
Adsorption

ABSTRACT

The adsorption of sulfur hexafluoride (SF_6) on multi-walled carbon nanotubes (MWNTs) was investigated. The properties of MWNTs were characterized and the adsorption capacities of SF_6 on MWNTs at different concentrations and temperatures were collected. H_2SO_4/H_2O_2 oxidation or KOH activation of MWNTs has effectively introduced the surface oxides and modified the microstructure without destruction of their graphitic crystalline structure. The MWNTs, especially the modified samples, are expected to be promising adsorbents for SF_6 removals from air. The saturated capacities of SF_6 with a concentration of 518 ppmv on the MWNTs ranged from 278 to 497 mg/g at 25 °C. The Toth equation has been reported to fit the adsorption data better than the Freundlich or Langmuir equation. The π–π dispersion interaction followed by the multi-layer adsorption and the electron donor–acceptor interaction were proposed to be the major adsorption mechanisms, depending on the adsorption temperature. The isosteric heat of adsorption, ranging from 51 to 124 kJ/mol with a loading of 30–300 mg/g, decreased with increasing SF_6 loading, reflecting the energetic heterogeneity of the MWNTs. These results suggest that the adsorption of SF_6 on MWNTs could be associated with binding to defect sites.

1. Introduction

Due to its low toxicity, thermal stability and high breakdown strength, sulfur hexafluoride (SF_6) is widely used in the electrical industry, semiconductor, aluminum smelting and magnesium industries, as well as medical applications [1]. In addition, SF_6 is also a common tracer gas for use in experiments or oceanography. But according to the Intergovernmental Panel on Climate Change, SF_6 is the most potent greenhouse gas with a global warming potential of 23,900 times that of CO_2 when compared over a 100-year period [2]. Due to the large amount produced annually and its long atmospheric lifetime (~3200 years), the use of SF_6 has recently become a global environmental issue.

SF_6 is a perfluorochemical (PFC) and there are several ways to reduce and eliminate PFC emissions from industrial processes. Because the process/equipment and material modifications are not currently practical, add-on-control approaches are the most available and cost-effective methods at present. Several studies have addressed the abatement/destruction methods such as thermal destruction [3], catalytic decomposition [4], plasma abatement [5], electrochemical reduction [6], photodegradation [7,8] and other advanced or combined abatement processes [9]. However, all of these are very costly and by-products emitted from some methods are harmful to human health and the environment [10]. The common techniques for recovery/recycling of SF_6 are cryogenic condensation, adsorption [11], and membrane separation [12]. In the late 1960s, a synthesized faujasite was used for SF_6 adsorption [13]. However, the carbonaceous adsorbents seemed to show a better performance for SF_6 adsorption [14]. The carbon black, activated carbons, carbon fabric and pillared clays have been used as adsorbents for SF_6 adsorption in the literature, and the SF_6 uptakes of as high as 800 mg/g of activated charcoal were observed [15–18].

Carbon nanotubes (CNTs) have attracted much attention for materials applications due to their unique mechanical, electrical, and gas storage properties. CNTs can be classified into single-walled carbon nanotubes (SWNTs) and multi-walled carbon nanotubes (MWNTs). Because of their light weight, small size, large surface area, and hollow geometry, CNTs have been considered as alternative materials for adsorption (storage), separation processes or as catalyst supports. These applications are highly dependent on the surface features and the pore size distribution of CNTs. Recently, SWNTs [19] or MWNTs [20] have been successfully used to remove many organic compounds from water.

The applications of gas adsorption originated with the removal of dioxins from air by MWNTs [21]. Studies on the adsorption of gases or vapors, such as hydrogen [22], methane [23], krypton [23,24], xenon [24], argon [25], toluene [26], methyl ethyl ketone [26], hexane [26], cyclohexane [26], benzene [27], thiophene [27,28], cyclohexane [27], and pentane [28] on SWNTs or methane [29], butane [30], krypton [31], ethylene [31], hydrogen [32], acetylene [33], trichloroethylene [34], benzene [34], n-hexane [34] and acetone [34] on MWNTs, have suggested that CNTs

* Corresponding author. Tel.: +886 3 4638800x2476; fax: +886 3 4558013.
E-mail address: ycchiang@saturn.yzu.edu.tw (Y.-C. Chiang).

0304-3894/$ – see front matter © 2010 Elsevier B.V. All rights reserved.
doi:10.1016/j.jhazmat.2010.02.003

may be suitable candidates as advanced adsorbents. The adsorptions of volatile organic compounds (VOCs) on SWNTs [26] and MWNTs [34] both were explored to be exothermic, namely increasing the temperature decreased the adsorption capacity. But the studies about the adsorption types and adsorption mechanisms indicated that investigating adsorption of specific compounds on a case by case basis is required. Agnihotri et al. [26] reported that the adsorption of *n*-hexane, cyclohexane, toluene and MEK on SWNTs was a typical physisorption. In other studies, the adsorption of trichloroethylene, benzene and *n*-hexane on MWNTs behaved physisorption [34,35], while acetone showed a chemisorption feature on MWNTs [34].

Several modification methods have been conducted to enhance the adsorption capacity of CNTs, especially using the chemical oxidation [19] or activation [36,37] treatment. Oxidative treatments may not always beneficially promote the adsorption of organic compounds on CNTs [19,38]. On the other hand, activation of CNTs usually is a promising approach for improving the adsorption capacity. The microporous cavities on MWNTs, the defects generated by KOH activation, enhanced the attraction force for hydrogen molecules [39]. Moreover, the hydrogen uptake of 4.47 wt% was achieved for KOH-modified MWNTs, where the residual potassium metal on the MWNTs was used to enhance physisorption of hydrogen gas [40].

The application of CNTs for adsorption of greenhouse gases has been investigated. For example, the CO_2 adsorption capacity of SWNTs has been reported to be twice as that of activated carbon [41] and the amine-modified MWNTs were recommended to be promising low-temperature adsorbents for CO_2 capture from flue gas [42]. In the applications of SF_6 adsorption, Muris et al. [11] reported that only one dense adsorbed layer of SF_6 can form on SWNTs and graphite before bulk condensation. The main differences of the adsorption on SWNTs with respect to the planar graphite are the increase of the condensation pressure and the decrease of the isosteric heat of adsorption (Q_{st}). In addition, the temperatures of the maximum rate of SF_6 desorption from the first monolayer on the graphite and SWNTs have been reported to be 100 and 150 °C, respectively [43], and the increase of desorption temperature on SWNTs has been attributed to physisorption in higher coordinated sites.

Although the adsorption performance of CNTs for SF_6 removal seems reasonable, there is little information on the adsorption equilibrium and thermodynamics, which is critical for evaluation and design of adsorption systems. Understanding adsorptive interactions between SF_6 and CNTs is of great importance to the environmental applications of CNTs as advanced adsorbents. This paper is concerned with the SF_6 adsorption on MWNTs that were modified by acid oxidation or KOH activation. MWNTs were used rather than SWNTs because MWNTs are less expensive. The properties of untreated or treated MWNTs were characterized, and the adsorption capacities of SF_6 on all MWNTs were collected. The Toth equation was found to fit the equilibrium data best, compared to the Langmuir and Freundlich equations. Then the Q_{st} was determined.

2. Experimental

2.1. Synthesis of MWNTs

The MWNTs were synthesized by chemical vapor deposition method through an iron catalyzed reaction in a tubular furnace system. Benzene was used as the carbon source, and ferrocene as the catalyst precursor. First, 0.1 g of ferrocene was vaporized in a quartz tube at 760 °C in flowing argon gas, and then benzene purged by argon gas (200 sccm) was directed into the quartz tube. The MWNT samples were obtained at 800 °C for 1 h. The pressure was maintained under 0.032 Torr for the whole process. The as-grown MWNT samples were purified by soaking in benzene solution for 24 h to eliminate carbonaceous impurities, and then treating by ultrasound for 1 h in 37 wt% HCl followed by the acid dissolution of catalyst particles for 6 h under stirring [44]. One commercial MWNT sample (Conyuan Biochemical Technology, Taiwan) was also obtained for comparison. The purified MWNT sample and the commercial product were denoted as NT1 and NT2, respectively.

2.2. Modifications of MWNTs

The MWNT samples were modified by means of wet chemical oxidation or chemical activation. A mixture of conc. H_2SO_4/H_2O_2 (4/1 by volume) was used to oxidize the MWNTs at 60 °C for 1 h [45]. After washing thoroughly with an excess of deionized water until the filtrate reached a pH value of ca. 7, the samples were dried at 103 °C in vacuum for 24 h. To ensure the samples were completely dried, the samples were heated to 450 °C at a heating rate of 20 °C/min in a nitrogen atmosphere for 4 h. The oxidized samples were denoted as NT1-so and NT2-so, respectively. Chemical activation with KOH was performed by an impregnation method [36,37]. The NT1 and NT2 were mixed with KOH solution at a KOH/CNT ratio of 4. Impregnation of 6 h was followed by drying the mixtures at 103 °C for 12 h to remove water. Then the dried mixtures were placed in a tubular furnace and heated to 850 °C in nitrogen flow with a heating rate of 5 °C/min for 1 h. After cooling, the activated samples were washed with HCl solution (1 M) and later with deionized water until the pH values of the filtrates were close to neutral. Then the samples were dried at 103 °C in vacuum for 24 h. The activated samples were denoted as NT1-a and NT2-a, respectively.

2.3. Characterization of MWNTs

High-resolution transmission electron microscopy (HRTEM) images of the MWNT samples were obtained by a transmission electron microscope (Philips, Tecnai G2, 200 kV) which was used to understand the interior microstructure of the MWNTs. X-ray diffraction (XRD) patterns were taken with an X-ray powder diffractometer (Japan MAC Science, MXP18). The radiation used was Cu K_α with a wavelength of 0.15418 nm. The 2-theta (2θ) ranged from 10° to 80°, where θ is the diffraction angle. Thermal analysis was carried out in a thermogravimetric analyzer (Dynamic TGA 2950 in TA Instrument 5100), measuring changes in the weight of a sample as a function of temperature (thermogravimetric analysis, TGA, plot) and the rate of weight loss versus temperature (differential thermogravimetry, DTG, plot). X-ray photoelectron spectroscopy (XPS) was employed to determine the chemical composition present on the outermost surface or at the tips of the MWNTs samples. The XPS spectra of all samples were acquired using a spectrophotometer (VG Scientific ESCALAB 210) with a microfocus monochromator Al K_α X-ray source ($h\nu$ = 1486.68 eV). The survey scan spectra were collected at the binding energy (B.E.) of 0–1000 eV with a step size of 1 eV, in order to identify the elements present on the MWNTs. The atomic ratios were calculated from the photoelectron peak area, using sensitivity factors according to the transmission characteristics of the Physical Electronics SCA.

The surface structure of MWNTs was examined by N_2 adsorption/desorption isotherms measured at −196 °C, carried out using a Micromeritics ASAP 2010 accelerated surface and porosimetry analysis system. Samples were outgassed at 350 °C overnight to remove adsorbed contaminants prior to the measurement. The specific surface area (SSA) of all samples was calculated using the standard Brunauer–Emmett–Teller (BET) method on eight points of the adsorption isotherm between $0.05 < P/P_0 < 0.2$. The total pore volume (V_t) was calculated by converting the amount adsorbed at a

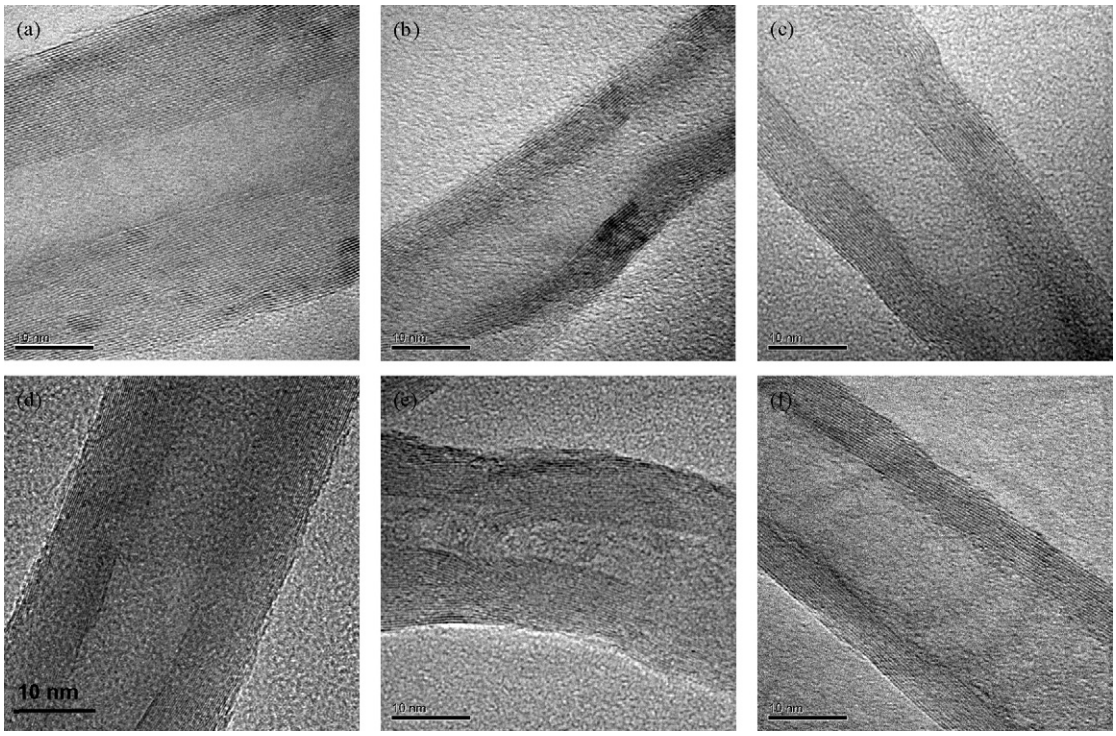

Fig. 1. HRTEM images of the MWNTs. (a) NT1; (b) NT1-so; (c) NT1-a; (d) NT2; (e) NT2-so and (f) NT2-a.

relative pressure of 0.99 to the volume of liquid adsorbate. Pore systems can be classified into three categories: macropore (>50 nm), mesopore (2–50 nm) and micropore (<2 nm) [46]. The micropore surface area (S_{mi}) and micropore volume (V_{mi}) were obtained by the *t*-plot method and HK method, respectively. The pore size distribution (PSD) curves of the MWNTs in the mesopore region were determined from the desorption branches of the isotherms using the BJH method [47,48]. At the scope of micropores, the HK model was used in place of the Kelvin equation [49].

2.4. SF_6 adsorption on MWNTs

The adsorption performance of SF_6 on MWNTs was determined by batch-equilibrium adsorption experiments. The MWNT sample (5 mg) was put into a 4-ml vial and placed in a 1-L laboratory bottle containing the SF_6 with the desired concentrations. In this study, the SF_6 concentrations were controlled at 65–15,000 ppmv by mixing pure SF_6 gas supplied by cylinders with nitrogen gas, measured by a thermal conductivity detector. The laboratory bottles then were sealed with Teflon-lined screw caps, and put in an incubator where the temperature was set at 5, 25, or 45 °C. The adsorption capacities of SF_6 on MWNTs at distinct temperatures and concentrations were determined by the gravimetric approach with a reaction time of 72 h to achieve the saturated adsorption. The time need for saturation, as well as the quality accuracy and quality control tests were also carried out in triplicate prior the experiments. Due to the reaction time for achieving the saturated adsorption was at least 72 h, the reproducibility tests were conducted for only one sample (NT2-a). The adsorption capacities of SF_6 with a concentration of 518 ppmv on NT2-a at different temperatures were gathered in triplicate, and the average adsorption capacities at 5, 25 and 45 °C were 812.2 ± 7.9, 499.7 ± 3.7 and 238.9 ± 7.2 mg/g, respectively.

In this study, the Freundlich, Langmuir and Toth equations were employed to fit the experimental data, and then to compare their goodness of fit. All estimated values of model parameters were determined by a commercial software program (KaleidaGraph). The Langmuir and Freundlich equations are the two most commonly applied models [19]. The Freundlich isotherm, Eq. (1), is an empirical equation that assumes heterogeneous adsorption due to the diversity of adsorption sites, as follows.

$$q_e = K_F C^{1/n} \tag{1}$$

where q_e (mg/g) is the equilibrium-adsorbed capacity, C (ppm) is the equilibrium gas phase concentration, K_F [(mg/g)(1/ppm)$^{1/n}$] is the Freundlich adsorption coefficient, and n is a constant indicating the isotherm curvature. The parameter n is usually greater than unity, and with larger values of n the adsorption isotherm becomes more nonlinear [50]. The parameters n and K_F usually both decrease with increasing temperature [51]. But the Freundlich equation has its limitations. That is, it does not have a proper Henry's law behavior at low pressure and it does not have a finite limit when the pressure is sufficiently high. In the Langmuir equation, Eq. (2),

$$q_e = \frac{q_o K_L C}{1 + K_L C} \tag{2}$$

q_o (mg/g) is the maximum adsorption capacity, and K_L (1/ppm) is the adsorption equilibrium constant. A large value of K_L implies strong bonding, i.e., large fractional surface coverage at a fixed temperature and concentration [51].

Another empirical equation that is popularly used and satisfies the two end limits is the Toth equation, which has the following form:

$$q_e = \frac{q_o C}{(b + C^t)^{1/t}} \tag{3}$$

where b (ppm^t) is the coefficient, and t is the degree of the heterogeneity of the adsorbent (usually less than unity) [50]. The parameters b and t are specific for adsorbate–adsorbent pairs. Since it is a three-parameter model, the Toth equation can describe many adsorption data well.

The heat of adsorption is a significant property for characterization of the type of adsorption and of the degree of heterogeneity of a surface [51]. The Q_{st} was calculated from the adsorption isotherms

at different temperatures using the Clausius–Clapeyron equation, Eq. (4),

$$\left(\frac{\partial \ln P}{\partial T}\right)_n = \frac{Q_{st}}{RT^2} \quad (4)$$

where P (N/m^2) is the equilibrium-adsorbed pressure, T (K) is the temperature, and R (=8.314 J/mol/K) is the gas constant. The calculated Q_{st} is sensitive to the choice of the isotherm equation [52]. For convenient use, Eq. (4) can be integrated and written as Eq. (5)

$$\ln P = A - \frac{Q_{st}}{R}\frac{1}{T} \quad (5)$$

where A is the constant of integration.

3. Results and discussion

3.1. HRTEM

The HRTEM images of the MWNTs samples are shown in Fig. 1. It can be seen that the outer layers of NT1 and NT2, with diameters of about 40 and 30 nm, have a nearly perfect graphitic layer structure (Fig. 1a and d). Some of the catalyst particles still remained in the ends of the tubes or in the hollow parts of the tubes (not shown here). However, the MWNTs modified by acid oxidation or KOH activation clearly showed morphological changes along the tube walls or at the tips under HRTEM study. Both treatments generated defective cylindrical graphene sheets or discontinuous graphene stack structures [32] and led to decrease in the number of graphene layers and the outer diameter (Fig. 1b, c, e and f). It is noteworthy that the KOH-activated samples had a significantly larger inner width (Fig. 1c and f), which indicates the inner tube walls were damaged by KOH in addition to the outer wall destruction. For MWNTs with smaller outside diameters, their specific surface areas and pore volumes are expected to be larger than those with larger outside diameters [30].

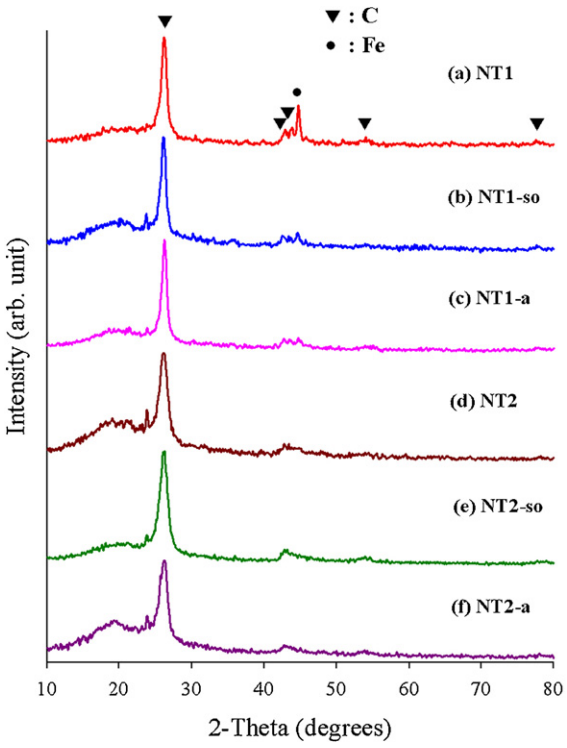

Fig. 2. XRD patterns of the MWNTs.

3.2. XRD

The XRD patterns of the NT1-series and NT2-series samples are shown in Fig. 2. The strongest and sharpest diffraction peak for all samples at around $2\theta = 26.2^\circ$ could be indexed as the C(0 0 2) reflection of graphite, and the other four characteristic diffraction peaks of graphite at 2θ of about 42.9°, 43.9°, 54.5° and 77.2° corresponded to C(1 0 0), C(1 0 1), C(0 0 4) and C(1 1 0), respectively. The

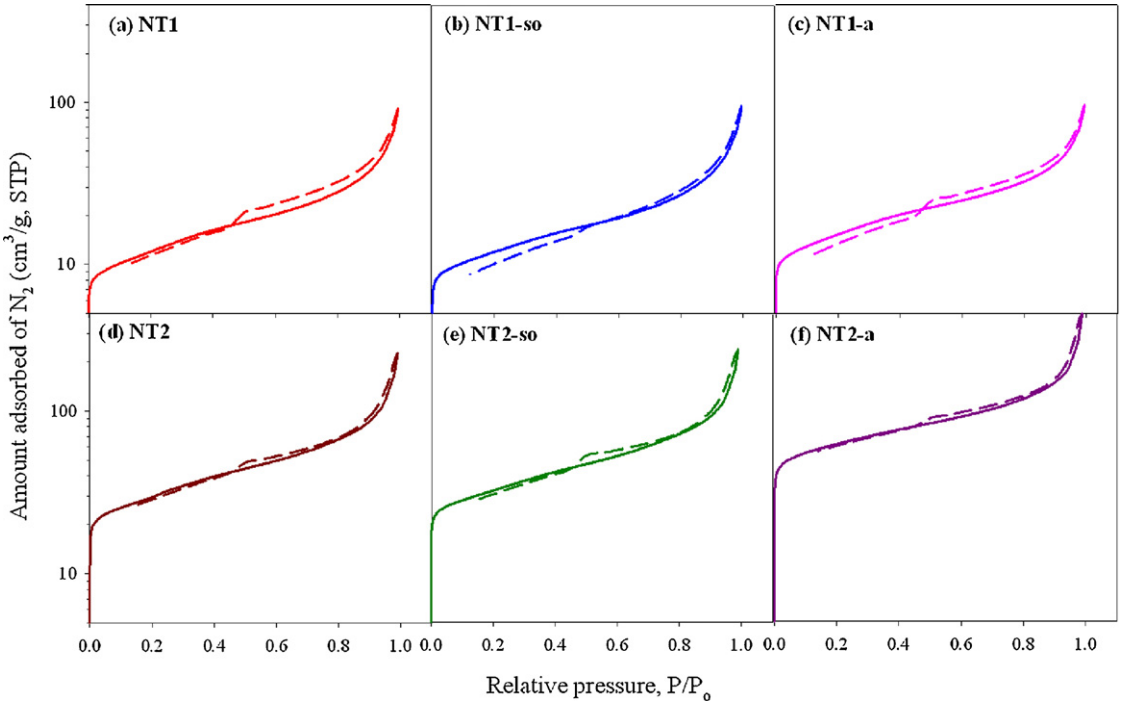

Fig. 3. Adsorption isotherms of nitrogen at −196 °C on the MWNT samples; solid lines represent the adsorption branch and dashed lines represent the desorption branch.

Table 1
Surface structure of the MWNTs determined from N_2 adsorption/desorption isotherms.

	SSA (m^2/g)	S_{mi}[a] (m^2/g)	S_{ext}[b] (m^2/g)	V_m (cm^3/g, STP)	V_t[c] (cm^3/g)	V_{mi}[d] (cm^3/g)	V_{me}[e] (cm^3/g)	V_{ma}[f] (cm^3/g)	Mean pore size[g] (nm)
NT1	43.07	0.13	42.94	9.89	0.1421	0.0122	0.0794	0.0505	13.20
NT1-so	42.61	3.94	38.67	9.79	0.1470	0.0122	0.0787	0.0561	13.80
NT1-a	54.89	7.45	47.44	12.61	0.1494	0.0156	0.0842	0.0496	10.89
NT2	104.73	6.27	98.46	24.06	0.3486	0.0307	0.2117	0.1062	13.31
NT2-so	115.21	17.76	97.45	26.47	0.3764	0.0354	0.2259	0.1151	13.07
NT2-a	218.21	53.95	164.26	50.13	0.6174	0.0657	0.3067	0.2450	11.32

[a] S_{mi} was determined by *t*-plot method.
[b] S_{ext} was obtained by subtracting S_{mi} from SSA.
[c] V_t represents the single point total pore volume at $P/P_o \approx 0.99$.
[d] V_{mi} was determined by HK method.
[e] V_{me} was calculated by BJH method.
[f] V_{ma} was found by subtracting V_{me} and V_{mi} from V_t.
[g] Mean pore size was obtained by $4V_t$/SSA.

sharpness of C(0 0 2) peaks indicated that the graphite structure of the MWNTs remained almost intact after modification. However, the interplanar spacing (d_{002}) calculated by Bragg's law decreased when the samples were oxidized by H_2SO_4/H_2O_2 mixture, implying that the removal of catalyst particles narrowed the spacing between graphitic layers. However, the d_{002} increased a little when the samples were activated by KOH, in agreement with Liu et al. [36]. It is expected that the MWNTs were intercalated by metallic K, which resulted in the separation and degradation of the graphene layers and followed the development of new defects [37]. The XRD analysis also provides evidence to identify the presence of the catalyst particles. There is one distinct diffraction peak at around $2\theta = 44.7^\circ$ in the XRD patterns of all samples, and one more weak peak at 2θ of about 65.0° was present in the XRD patterns of NT1 and NT2. The results of energy dispersive spectroscopy (EDS) confirmed the presence of Fe, and so the diffraction peaks at around $2\theta = 44.7^\circ$ and 65.0° were assigned to Fe(1 1 0) and Fe(2 0 0).

3.3. Surface structure

Fig. 3 shows N_2 adsorption/desorption isotherms of the MWNTs at −196 °C, where the amount of N_2 adsorbed is shown on a log scale in the figure so that the shape of the adsorption curves at low pressures can be seen more readily. It can be seen that the adsorption isotherms were essentially between type II and type IV of the BET classification. Even so, there is a slightly larger amount of adsorption on the KOH-activated samples at low pressures, representing the presence of micropores through KOH activation.

It is known that the open state of the CNTs is an essential factor for the presence of the hysteresis loop. The existence of a clear hysteresis loop over P/P_o >0.45 in all MWNTs implies that some tubes had two accessible ends [29] and the MWNTs could be regarded as mesoporous materials [53]. Based on the classification recommended by IUPAC [54], the hysteresis loops of the MWNT samples were recognized as type H3, which is characterized by slit-shaped pores, in contrast to the results of Liu et al. [47]. It is noteworthy that the hysteresis loops of NT2-series samples all displayed a contraction near P/P_o ~0.8 for NT2 and NT2-so and P/P_o ~0.87 for NT2-a, which was reported in our previous study [55]. The capillary condensation occurring in the first section of the hysteresis loop over P/P_o = 0.45–0.80 or 0.45–0.87 (~pore size of 3.7–10.5 or 3.7–16.5 nm) probably implied adsorption in inner diameter of the opened MWNTs. This assumption has been verified by the HRTEM images, where the tubular structure was not changed very much after oxidation, but the inner diameter was significantly enlarged due to KOH activation. As for the hysteresis loop over P/P_o of 0.8 or 0.87, it was expected to be partially caused by the aggregated pores formed by the confined space among the entangled MWNTs [56]. This conclusion also can be supported by the behavior that the desorption branch was below the adsorption branch in some

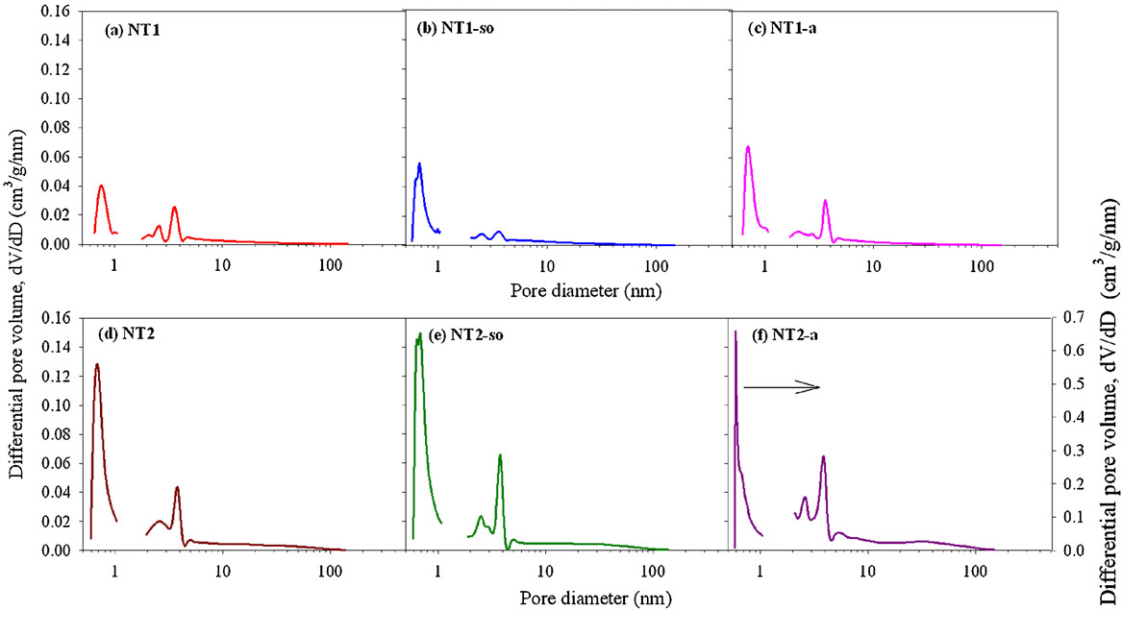

Fig. 4. PSD curves of the MWNTs.

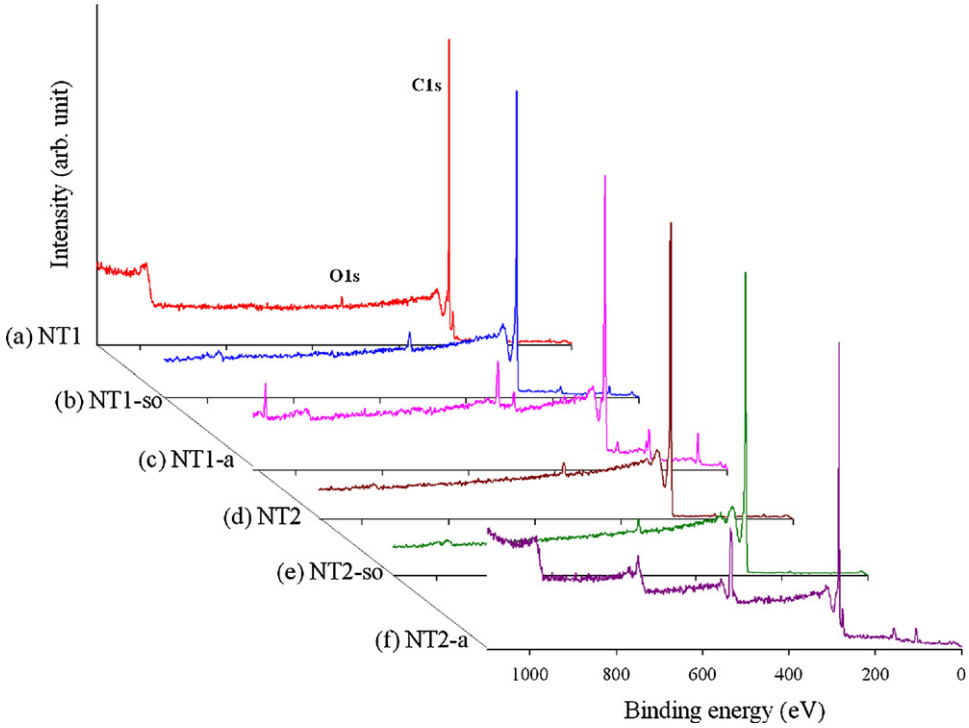

Fig. 5. XPS survey scan spectra of the MWNTs.

samples, which means the structure had changed after N_2 adsorption/desorption processes.

Table 1 lists the surface structure data for all MWNT samples, where the BET model was applied to yield the adsorbed amount of monolayer (V_m) and the SSA. The SSA and V_t of NT2 were approximately 2.4 times those corresponding to NT1. H_2SO_4/H_2O_2 oxidation or KOH activation has significantly increased the S_{mi} and V_t, especially for KOH activation. The percents of mesopore volume (V_{me}) and macropore volume (V_{ma}) for all samples ranged from 50% to 61% and 30% to 40%, indicative of the mesoporous materials even with modifications, though the percent of V_{mi} increased to over 10% of V_t after KOH activation.

The development of porosity after modifications could be recognized from the PSD curves, shown in Fig. 4, where curves in the mesoporous region were calculated by the BJH method and those in the microporous region were obtained by the HK method. Patterns of PSD curves for two series samples were similar, but the differential pore volumes for NT2-series were much greater than those for NT1-series. There were three distinct peaks in all curves, wherein the peak at about 0.7 nm should be the small defect sites appeared on the wall or at the opened ends of the nanotubes while the other two peaks at around 2.6 and 3.6–3.9 nm were expected to be the inside diameters of the nanotubes [57]. The PSD curve over 4 nm should be the contribution from the intertubular spaces of the aggregated MWNTs [58]. Consequently, both modifications showed the ability for generation of new pores on nanotubes, and KOH activation was more effective than acid oxidation.

3.4. XPS

Fig. 5 shows the XPS survey scan spectra of as-received and treated MWNTs, which reveals the compositions of the most external surface of the nanotubes. The major peaks observed in the scan spectra were due to the C1s and O1s photoelectrons. The O/C atomic ratios derived from survey scan spectra were compared to determine the effects of various treatments. For NT1 and NT2, the O/C ratios were 0.018 and 0.022, respectively. After oxidation with conc. H_2SO_4/H_2O_2 solution, the O/C ratios increased to 0.034 and 0.031. It is interesting that the KOH activation evidently introduced a considerable amount of surface oxides onto the MWNTs in addition to increase in porosity, in agreement with Liu et al. [36]. The O/C ratios of NT1-a and NT2-a were highly promoted, up to 0.167 and 0.204, respectively, both with about a ninefold enhancement compared to the untreated samples. It is expected that the defects formed on MWNTs during KOH activation were active to attach oxygen-containing functional groups.

3.5. TGA–DTG

The TGA–DTG profiles measured in flowing air for all samples are shown in Fig. 6. The temperatures of the maximum rate of weight loss (or oxidation) for NT1, NT1-so, and NT1-a were 669.8, 649.3, and 634.2 °C, while the corresponding NT2-series were 689.8, 701.0 and 613.3 °C, respectively. As seen from the data, the maximum rate of weight loss took place at lower temperatures as the samples were activated by KOH, which implies that the thermal stability of MWNTs was destroyed because of the increase in porosity and decrease in graphene layers. However, the effect of acid oxidation was not in agreement on NT1 and NT2. It is believed that the oxidation of H_2SO_4/H_2O_2 exposed the catalysts because the outer graphene layers were oxidized, but this oxidation was unable to eliminate the catalysts completely. This conclusion was verified by the TGA residue (shown in Fig. 6). Therefore, the oxidized samples containing higher residual Fe were unstable and had a lower temperature for the maximum rate of weight loss. It is noteworthy that very high values of residue were measured on KOH-activated samples, 6.9% for NT1-a and 9.4% for NT2-a. This result was considered to be the intercalation of metallic K within the graphene layers and was confirmed by the EDS analysis (not shown here).

3.6. Adsorption of SF_6

The experimental equilibrium data of SF_6 collected on all MWNT samples at different concentrations and temperatures are shown in

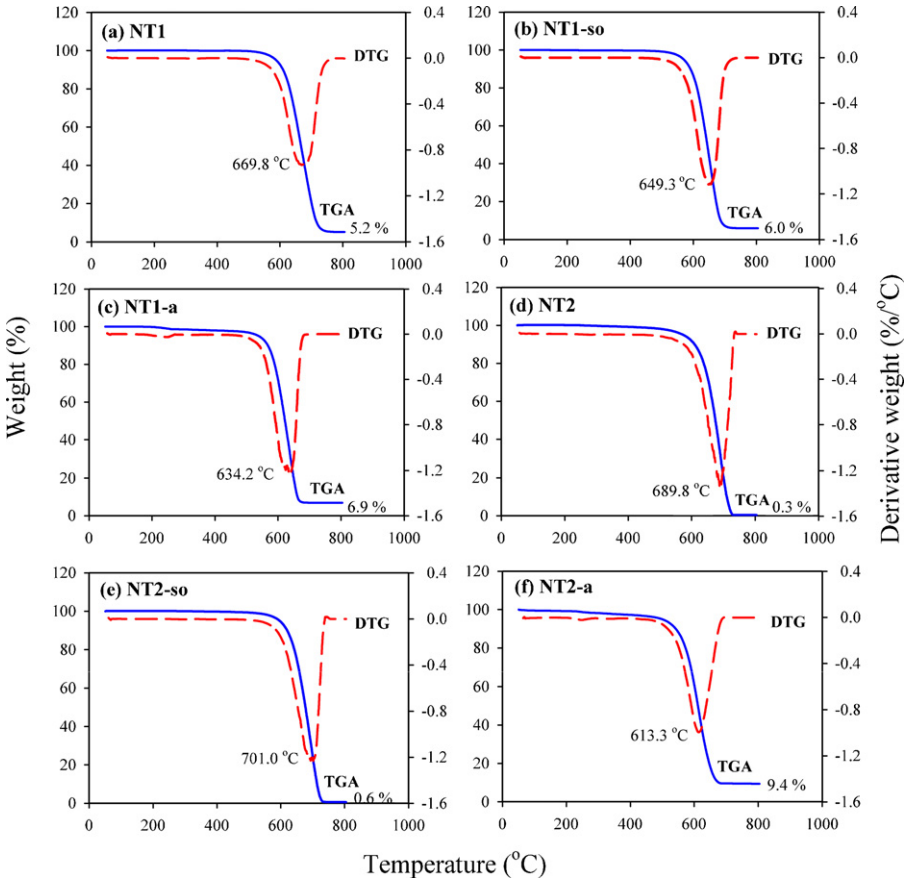

Fig. 6. TGA/DTG profiles of the MWNTs, where the samples were heated at a rate of 10 °C/min in the air flow of 50 cm^3/min.

Fig. 7 and Table 2. Compared to other adsorbents in the literature [13–18], the MWNTs should be a promising candidate as adsorbents for SF_6 adsorption. It is clear that the adsorbed amount decreased with increasing temperature, indicative of exothermic adsorption. SF_6 is a hypervalent molecule with six bonding pairs, and the free SF_6 molecule has been found to be a regular octahedron and can be inscribed in a sphere of 0.56 nm diameter [11]. Therefore, it was expected that most of the SF_6 molecules were adsorbed on the

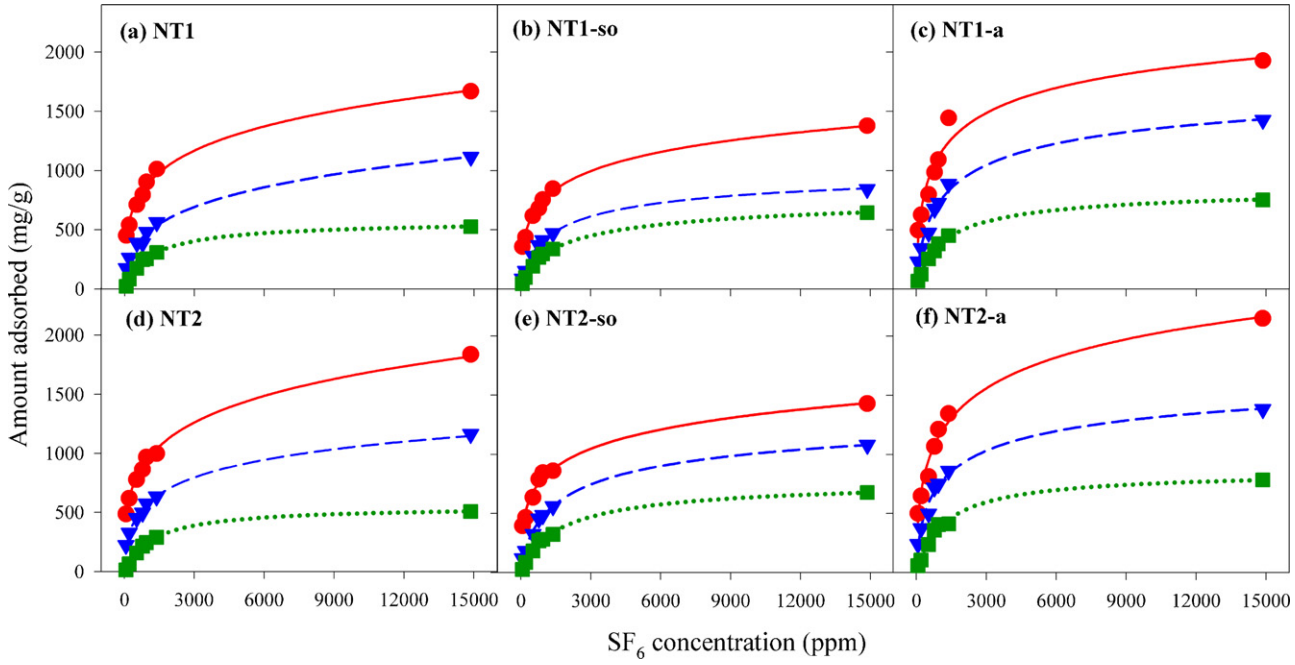

Fig. 7. Adsorption isotherms of SF_6 on MWNTs at (●) 5 °C, (▼) 25 °C and (■) 45 °C. Lines represent the model fittings of the Toth equation.

Table 2
Adsorption capacities of SF_6 on the MWNTs used in this study.

Concentration (ppmv)	Adsorption capacity (mg/g)								
	NT1			NT1-so			NT1-a		
	5 °C	25 °C	45 °C	5 °C	25 °C	45 °C	5 °C	25 °C	45 °C
65	451	174	21	357	86	43	496	231	67
200	541	260	83	437	150	96	627	343	125
518	711	387	174	618	278	191	799	474	254
772	795	384	246	681	367	264	986	675	322
939	904	479	254	755	409	295	1092	726	382
1376	1013	563	308	846	469	337	1445	886	450
14,863	1670	1114	525	1378	841	644	1928	1425	753
Concentration (ppmv)	NT2			*NT2 − so*			NT2-a		
	5 °C	25 °C	45 °C	5 °C	25 °C	45 °C	5 °C	25 °C	45 °C
65	486	222	13	395	119	26	500	240	59
200	619	325	65	465	181	85	647	373	106
518	777	450	157	636	323	181	812	497	237
772	863	496	215	788	454	268	1069	718	358
939	968	573	245	846	483	280	1213	749	405
1376	998	633	290	859	559	322	1346	860	411
14,863	1837	1163	507	1430	1079	675	2150	1383	783

external surface of the MWNTs and only a small fraction of the SF_6 molecule condensed in the pores because the latter process would take longer [30].

Table 3 lists the isotherm parameters derived from the Langmuir, Freundlich and Toth equations for the data of SF_6 adsorbed on all MWNT samples. The *R*-square (R^2) values were used to measure how successful the fit was in explaining variations of the data. Comparing the model fittings of the Langmuir equation with the Freundlich equation, it is clear that the Freundlich equation was more suitable to describe the SF_6 adsorption on MWNTs at lower temperature (5 °C) and the system where the MWNTs had fewer surface functional groups. On the other hand, the Langmuir equation fitted the experimental data much better than the Freundlich model when adsorption occurred at 45 °C and the system where the MWNTs had more surface functional groups.

As can be seen from Table 3, the Toth equation had the best fit for all of the isotherms, supported by the high R^2 values between 0.948 and 0.997, despite the fact that the Langmuir and Freundlich equations are more widely used. Consequently, the Toth equation was suggested to describe the adsorption data in this study and the model fittings are also presented in Fig. 7. The Toth model is a three-parameter equation, so this model could provide more information about the adsorption system. When the parameter *t* is unity, the Toth equation reduces to the Langmuir equation, and when it deviates further from unity, the system is said to be more heterogeneous [50]. Accordingly, all isotherms at 5 °C were deviated from the Langmuir type because the *t* values ranged from 0.094 to 0.253, with the order NT < NT-so < NT-a for both series. This implies the multi-layer adsorptions at lower temperatures. At room temperature (25 °C), NT1 and NT2 were much more heterogeneous than the other samples, and the *t* values followed the order NT ≪ NT-a < NT-so. This indicates that the existence of surface oxides would prompt the adsorption phenomenon toward the monolayer adsorption at room temperatures. However, the formation of new pores could conflict with this action. Under 45 °C, all isotherms were close to the Langmuir type because the *t* values approached unity very well, following the order NT-so < NT-a < NT < 1. This indicates that the monolayer adsorption was predominant at higher temperatures. This finding coincided very well with the previous discussion. That is, the experimental data can be fitted well by a Langmuir equation

Table 3
Coefficients of the model fittings for adsorption of SF_6 on MWNTs at different temperatures (*T*).

Sample	*T* (°C)	Langmuir			Freundlich			Toth					
		q_o (mg/g)	K_L (10^{-4}/ppm)	R^2	K_F ((mg/g)(1/ppm)$^{1/n}$)	*n*	R^2	q_o (mg/g)	*b* (ppm^t)	*t*	R^2	ln *H* (mg/g/ppm)	Q_{st}^o (kJ/mol)
NT1	5	1661.0	14.6	0.849	161.7	4.1	0.989	20,991.0	0.67	0.094	0.991	14.27	271.6
	25	1191.4	7.6	0.942	49.3	3.1	0.991	13,779.0	1.32	0.129	0.993	7.37	
	45	565.0	8.9	0.998	24.2	3.1	0.914	581.8	468.98	0.888	0.997	−0.56	
NT1-so	5	1366.1	15.4	0.874	137.5	4.1	0.987	3723.9	1.43	0.197	0.994	6.41	119.9
	25	899.8	8.7	0.994	40.3	3.1	0.952	1093.8	41.38	0.580	0.996	0.57	
	45	698.9	7.5	0.997	24.0	2.9	0.952	850.2	58.25	0.602	0.997	−0.01	
NT1-a	5	1968.4	16.2	0.895	211.9	4.3	0.916	2975.7	4.10	0.341	0.948	3.86	70.8
	25	1501.6	10.6	0.970	93.3	3.5	0.949	1962.6	16.64	0.481	0.984	1.74	
	45	808.2	9.1	0.998	37.4	3.2	0.929	870.3	175.90	0.765	0.997	0.01	
NT2	5	1809.9	13.8	0.808	167.2	4.0	0.997	19,597.0	0.72	0.101	0.994	13.07	256.4
	25	1197.9	10.5	0.919	77.4	3.5	0.993	2678.3	2.82	0.256	0.995	3.84	
	45	551.3	8.0	0.997	19.8	2.9	0.913	553.0	1113.00	0.986	0.997	−0.80	
NT2-so	5	1394.9	17.7	0.859	159.5	4.3	0.976	4304.0	1.13	0.174	0.986	7.69	153.6
	25	1164.0	7.6	0.989	43.7	3.0	0.967	1493.1	35.51	0.543	0.996	0.74	
	45	744.5	6.3	0.996	19.1	2.7	0.957	797.6	358.69	0.813	0.996	−0.56	
NT2-a	5	2190.0	13.6	0.914	192.4	3.9	0.964	4571.7	2.36	0.253	0.980	5.03	97.4
	25	1431.0	12.4	0.962	107.3	3.7	0.948	1936.6	10.82	0.440	0.986	2.16	
	45	842.8	8.4	0.988	33.7	3.0	0.925	860.3	646.99	0.922	0.988	−0.27	

when t was greater than 0.4. As t was less than 0.4, the Freundlich-type isotherms would be more acceptable. Based on the above discussion, in addition to the adsorbents, the adsorption temperature seemed to have much more influence on the parameter t. It can be seen that the t values for NT1 and NT2 changed substantially as the temperature increased from 5 to 45 °C. However, the temperature effect was moderated on treated samples. This result indicates that the modification of MWNTs should be necessary for their applications since they can then be more widely suitable for use.

The fitted parameter q_o is unusually large at 5 and 25 °C for untreated samples, reflecting the Freundlich-type character. The adsorption at 5 °C indicated that the surface oxides on the tube walls were expected to create polar region, reducing the surface area available for adsorption [59]. Accordingly, the π–π dispersion interaction followed by multi-layer adsorption could be the main adsorption mechanisms at 5 °C. When the temperature increased, in addition to the π–π dispersion interaction, the surface oxides may be active to affect the adsorption affinity of SF_6 onto MWNTs. SF_6 is a nonpolar molecule, which can act as an electron acceptor [60] when interacting with the MWNTs containing structures with electron donors such as surface oxides. Referring to the fitted parameters, the electron donor–acceptor interaction mechanism was expected to function at 25 °C. Moreover, this mechanism took over to control the adsorption system at 45 °C.

The Henry's law constant (H) for the Toth equation shown in Eq. (6) can be used to estimate the isosteric heat of adsorption at zero loading (Q_{st}^o).

$$H = q_o b^{-1/t} \tag{6}$$

The Q_{st}^o is often used as a parameter to characterize adsorption energetics. By plotting ln(H) against $1/T$, the Q_{st}^o is derived from the slope. The H value for each system is also listed in Table 3. All Q_{st}^o were in the range of 70–272 kJ/mol, which is significantly higher than the values reported for physical adsorption of VOCs by conventional carbon materials. A high Q_{st}^o value of 41.5 kJ/mol was also reported for the case of SF_6 adsorption on a molecular sieving carbon [16]. The interactions between a graphitic carbon surface and an adsorbed molecule would increase as the surface becomes highly curved [30]. For both series of samples, the values of Q_{st}^o followed the order NT-a < NT-so < NT. The decrease in wall number may be one of the reasons that KOH-activated samples had the lowest Q_{st}^o. Moreover, this result also indicates that although the surface oxides on KOH-activated samples could derive the electron donor–acceptor interactions, their space obstacles mitigated the adsorption affinity for SF_6 due to its large molecule size. Consequently, NT1 and NT2, which preserved a prefect graphene structure, presented a stronger adsorption affinity for SF_6.

The nature and degree of heterogeneity of the adsorbent very strongly influenced the isosteric heats of adsorbates [61]. The Q_{st} at other surface loadings were calculated using the Clausius–Clapeyron equation (Eq. (5)) with the fitted Toth isotherms, which were plotted in Fig. 8a. As seen from this figure, the value of Q_{st} decreased as surface loading increased. If the Q_{st} was plotted against the amount adsorbed shown on a log scale (Fig. 8b), good linearity of the plot was observed. The dependence of the Q_{st} values on loading is an indication that the MWNTs exhibited significant energetic heterogeneity and the adsorption of SF_6 molecules occurred on different adsorption sites. Initial high Q_{st} values were due to adsorption on the highest energy sites; when these became saturated adsorption proceeded to sites of lower adsorption energy which corresponded to a decrease in Q_{st} [17]. The variation of Q_{st} versus the loading was similar to those published in the literature with carbonaceous materials as adsorbents for SF_6 adsorption [14–16], though the values of Q_{st} in this study were much higher

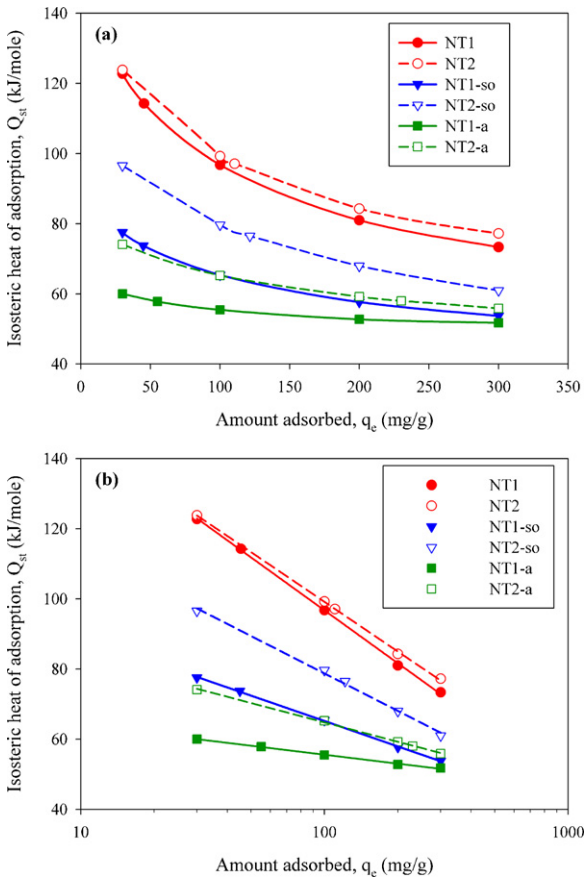

Fig. 8. Isosteric heat of adsorption as a function of the amount of SF_6 adsorbed on MWNT samples.

than those of conventional physisorption. Similar high levels of Q_{st} were also observed in VOCs adsorption on SWNTs [26], where increasing the dipole moments of VOCs decreased the Q_{st} values. When comparing results at a loading of 50 mg/g, the Q_{st} of hexane on SWNTs (256.3 kJ/mol) [26] was more than twice the values presented in this study. This finding suggests that the SF_6 adsorption on MWNTs was associated with binding to defect sites [43].

4. Conclusions

Both acid oxidation and KOH activation of the MWNTs generated defective cylindrical graphene structure, eliminated the catalyst particles, modified the interplanar spacing, introduced the surface oxides, and decreased the number of graphene layers, especially for the KOH-activated samples. These modifications made the MWNTs more active. The PSD curves of the MWNTs were three-modal, indicating the defect sites and the inside diameters of the nanotubes. The adsorption of SF_6 on MWNTs was exothermic reactions and showed a well-behaved chemisorption. The Toth equation fitted the adsorption data better than the Freundlich and Langmuir equations. At low adsorption temperatures, the MWNTs were more heterogeneous and the π–π dispersion interaction followed by the multi-layer adsorption was the major adsorption mechanisms. The electron donor–acceptor interaction was expected to function at room temperature, and this mechanism took over to control the adsorption system at 45 °C because the samples became more homogeneous and the monolayer adsorption was predominant. The values of the isosteric heat of adsorption at zero loading were influenced by the number of wall layers and the surface oxides. Moreover, the value of isosteric heat of adsorption decreased as surface loading increased, and a good linear relationship was observed.

In this study, the modification of MWNTs is suggested for their application and the MWNTs have been proven to be excellent adsorbents for the removal of SF_6 from air.

Acknowledgement

The authors gratefully thank the National Science Council (NSC) of Taiwan for financial support, through Project No. NSC 96-2211-E-155-003.

References

[1] M. Maiss, C.A.M. Brenninkmeijer, Atomspheric SF_6: trends, sources and prospects, Environ. Sci. Technol. 32 (1998) 3077–3086.
[2] V. Mohindra, H. Chase, H.H. Sawin, M.T. Mocella, Abatement of perfluorocompounds (PFCS) in a microwave tubular reactor using O_2 as an additive gas, IEEE Trans. Plasma Sci. 10 (1997) 399–407.
[3] J. McNabb, S. Bischke, Optimization of C_2F_6 burnbox destruction, Semicond. Int. 21 (1998) 131–134.
[4] Y. Takita, C. Morita, M. Ninomiya, H. Wakamatsu, H. Nishiguchi, T. Ishihara, Catalytic decomposition of CF_4 over $AlPO_4$-based catalysts, Chem. Lett. 5 (1999) 417–418.
[5] C.H. Tsai, J.M. Shao, Formation of fluorine for abating sulfur hexafluoride in an atmospheric-pressure plasma environment, J. Hazard. Mater. 157 (2008) 201–206.
[6] R. Taylor-Smith, Electrochemical routes to perfluorocompound abatement, Electrochem. Soc. Proc. 99-8 (1999) 116–125.
[7] L. Huang, Y. Shen, W. Dong, R. Zhang, J. Zhang, H. Hou, A novel method to decompose two potent greenhouse gases: photoreduction of SF_6 and SF_5CF_3 in the presence of propene, J. Hazard. Mater. 151 (2008) 323–330.
[8] X. Song, X. Liu, Z. Ye, J. He, R. Zhang, H. Hou, Photodegradation of SF_6 on polyisoprene surface: implication on elimination of toxic byproducts, J. Hazard. Mater. 168 (2009) 493–500.
[9] M. Radoiu, S. Hussain, Microwave plasma removal of sulphur hexafluoride, J. Hazard. Mater. 164 (2009) 39–45.
[10] W.T. Tsai, The decomposition products of sulfur hexafluoride (SF_6): reviews of environmental and health risk analysis, J. Fluorine Chem. 128 (2007) 1345–1352.
[11] M. Muris, N. Dupont-Pavlovsky, M. Bienfait, P. Zeppenfeld, Where are the molecules adsorbed on single-walled nanotubes? Surf. Sci. 492 (2001) 67–74.
[12] W.T. Tsai, H.P. Chen, W.Y. Hsien, A review of uses, environmental hazards and recovery/recycle technologies of perfluorocarbons (PFCs) emissions from the semiconductor manufacturing processes, J. Loss Prev. Process Ind. 15 (2002) 65–75.
[13] J.K. Thompson, H.A. Resing, A study of surface diffusion by NMR: sulfur hexafluoride adsorbed on synthetic faujasite, J. Colloid Interface Sci. 26 (1968) 279–286.
[14] D.V. Cao, S. Sircar, Heat of adsorption pf pure sulfur hexafluoride on micromesoporous adsorbents, Adsorption 7 (2001) 73–80.
[15] E.L. Fuller Jr., S.D. Clinton, K.J. Fallon, C.M. Jones, J.J. Perona, J.S. Watson, S.M. Senkan, Sorption of SF_6 by activated charcoal, J. Chem. Eng. Data 26 (1981) 4–7.
[16] J. Jagiełło, T.J. Bandosz, K. Putyera, J.A. Schwarz, Adsorption near ambient temperatures of methane, carbon tetrafluoride, and sulfur hexafluoride on commercial activated carbons, J Chem. Eng. Data 40 (1995) 1288–1292.
[17] T.J. Bandosz, J. Jagiełło, J.A. Schwarz, Adsorption of sulfur hexafluoride and propane at temperatures near ambient on pillared clays, J. Chem. Eng. Data 41 (1996) 880–884.
[18] A.A. Pribylov, I.A. Kalinnikova, N.I. Regent, Features of sulfur hexafluoride adsorption on carbon adsorbents, Russ. Chem. Bull. 52 (2003) 882–888.
[19] X.E. Shen, X.Q. Shan, D.M. Dong, X.Y. Hua, G. Owens, Kinetics and thermodynamics of sorption of nitroaromatic compounds to as-grown and oxidized multiwalled carbon nanotubes, J. Colloid Interface Sci. 330 (2009) 1–8.
[20] G.C. Chen, X.Q. Shan, Y.Q. Zhou, X.E. Shen, H.L. Huang, S.U. Khan, Adsorption kinetics, isotherms and thermodynamics of atrazine on surface oxidized multiwalled carbon nanotubes, J. Hazard. Mater. 169 (2009) 912–918.
[21] R.Q. Long, R.T. Yang, Carbon nanotubes as superior sorbent for dioxin removal, J. Am. Chem. Soc. 123 (2001) 2058–2059.
[22] Y. Ye, C.C. Ahn, C. Witham, B. Fultz, J. Liu, A.G. Rinzler, D. Colbert, K.A. Smith, R.E. Smalley, Hydrogen adsorption and cohesive energy of single-walled carbon nanotubes, Appl. Phys. Lett. 74 (1999) 2307–2309.
[23] M. Muris, N. Dufau, M. Bienfait, N. Dupont-Pavlovsky, Y. Grillet, J.P. Palmari, Methane and krypton adsorption on single-walled carbon nanotubes, Langmuir 16 (2000) 7019–7022.
[24] M.R. Babaa, I. Stepanek, K. Masenelli-Varlot, N. Dupont-Pavlovsky, E. McRae, P. Bernier, Opening of single-walled carbon nanotubes: evidence given by krypton and xenon adsorption, Surf. Sci. 531 (2003) 86–92.
[25] Z.J. Jakubek, B. Simard, Two confined phases of argon adsorbed inside open single walled carbon nanotubes, Langmuir 20 (2004) 5940–5945.
[26] S. Agnihotri, M.J. Rood, M. Rostam-Abadi, Adsorption equilibrium of organic vapors on single-walled carbon nanotubes, Carbon 43 (2005) 2379–2388.
[27] D. Crespo, R.T. Yang, Adsorption of organic vapors on single-walled carbon nanotubes, Ind. Eng. Chem. Res. 45 (2006) 5524–5530.
[28] J. Goering, U. Burghaus, Adsorption kinetics of thiophene on single-walled carbon nanotubes (CNTs), Chem. Phys. Lett. 447 (2007) 121–126.
[29] E.B. Mackie, R.A. Wolfson, L.M. Arnold, K. Lafdi, A.D. Migone, Adsorption studies of methane films on catalytic carbon nanotubes and on carbon filaments, Langmuir 13 (1997) 7197–7201.
[30] J. Hilding, E.A. Grulke, S.B. Sinnott, D. Qian, R. Andrews, M. Jagtoyen, Sorption of butane on carbon multiwall nanotubes at room temperature, Langmuir 17 (2001) 7540–7544.
[31] K. Masenelli-Varlot, E. McRae, N. Dupont-Pavlovsky, Comparative adsorption of simple molecules on carbon nanotubes: dependence of the adsorption properties on the nanotube morphology, Appl. Surf. Sci. 196 (2002) 209–215.
[32] P.X. Hou, S.T. Xu, Z. Ying, Q.H. Yang, C. Liu, H.M. Cheng, Hydrogen adsorption/desorption behavior of multi-walled carbon nanotubes with different diameters, Carbon 41 (2003) 2471–2476.
[33] G. Onyestyák, J. Valyon, K. Hernádi, I. Kiricsi, L.V.C. Rees, Equilibrium and dynamics of acetylene sorption in multiwalled carbon nanotubes, Carbon 41 (2003) 1241–1248.
[34] Y.H. Shih, M.S. Li, Adsorption of selected volatile organic vapors on multiwall carbon nanotubes, J. Hazard. Mater. 154 (2008) 21–28.
[35] E. Díaz, S. Ordóñez, A. Vega, Adsorption of volatile organic compounds onto carbon nanotubes, carbon nanofibers, and high-surface-area graphites, J. Colloid Interface Sci. 305 (2007) 7–16.
[36] Y. Liu, Z. Shen, K. Yokogawa, Investigation of preparation and structures of activated carbon nanotubes, Mater. Res. Bull. 41 (2006) 1503–1512.
[37] E. Raymundo-Piñero, P. Azaïs, T. Cacciaguerra, D. Cazorla-Amorós, A. Linares-Solano, F. Béguin, KOH and NaOH activation mechanisms of multiwalled carbon nanotubes with different structural organization, Carbon 43 (2005) 786–795.
[38] C.J.M. Chin, L.C. Shih, H.J. Tsai, T.K. Liu, Adsorption of o-xylene and p-xylene from water by SWNTs, Carbon 45 (2007) 1254–1260.
[39] C.H. Chen, C.C. Huang, Hydrogen adsorption in defective carbon nanotubes, Sep. Purif. Technol. 65 (2009) 305–310.
[40] C.H. Chen, C.C. Huang, Hydrogen storage by KOH-modified multi-walled carbon nanotubes, Int. J. Hydrogen Energy 32 (2007) 237–246.
[41] M. Cinke, J.L. Charles, W. Bauschlicher Jr., A. Ricca, M. Meyyappan, CO_2 adsorption in single-walled carbon nanotubes, Chem. Phys. Lett. 376 (2003) 761–766.
[42] F. Su, C. Lu, W. Cnen, H. Bai, J.F. Hwang, Capture of CO_2 from flue gas via multiwalled carbon nanotubes, Sci. Total Environ. 407 (2009) 3017–3023.
[43] H. Ulbricht, R. Zacharia, N. Cindir, T. Hertel, Thermal desorption of gases and solvents from graphite and carbon nanotube surfaces, Carbon 44 (2006) 2931–2942.
[44] F. Li, H.M. Cheng, Y.T. Xing, P.H. Tan, G. Su, Purification of single-walled carbon nanotubes synthesized by the catalytic decomposition of hydrocarbon, Carbon 38 (2000) 2041–2045.
[45] D. Bonifazi, C. Nacci, R. Marega, S. Campidelli, G. Ceballos, S. Modesti, M. Meneghetti, M. Proto, Microscopic and spectroscopic characterization of paintbrush-like single-walled carbon nanotubes, Nano Lett. 6 (2006) 1408–1414.
[46] IUPAC Manual of Symbols and Terminology, 1972.
[47] Z.T. Liu, C.X. Wang, Z.W. Liu, J. Lu, Selective hydrogenation of cinnamaldehyde over Pt-supported multi-walled carbon nanotubes: insights into the tube-size effects, Appl. Catal. A 344 (2008) 114–123.
[48] L. Li, G. Wu, B.Q. Xu, Electro-catalytic oxidation of CO on Pt catalyst supported on carbon nanotubes pretreated with oxidative acids, Carbon 44 (2006) 2973–2983.
[49] F. Li, Y. Wang, D. Wang, F. Wei, Characterization of single-wall carbon nanotubes by N_2 adsorption, Carbon 42 (2004) 2375–2383.
[50] D.D. Do, Adsorption Analysis: Equilibria and Kinetics Series on Chemical Engineering, vol. 2, Imperial College Press, London, 1998.
[51] C.N. Satterfield, Heterogeneous Catalysis in Industrial Practice, second ed., McGraw-Hill, New York, 1993.
[52] K. Wang, S. Qiao, X. Hu, Study of isosteric heart of adsorption and activation energy for surface diffusion of gases on activated carbon using equilibrium and kinetics information, Sep. Purif. Technol. 34 (2004) 165–176.
[53] S. Inoue, N. Ichikuni, T. Susuki, T. Uematsu, K. Kaneko, Capillarity condensation of N_2 on multiwall carbon nanotubes, J. Phys. Chem. B 102 (1998) 4689–4692.
[54] V.P. Zhdanov, Application of percolation theory to describing kinetic processes in porous solids, Adv. Catal. 39 (1993) 1–50.
[55] Y.C. Chiang, C.Y. Lee, Changes in material properties and surface fractality of multi-walled carbon nanotubes modified by heat and acid treatments, J. Mater. Sci. 44 (2009) 2780–2791.
[56] Q.H. Yang, P.X. Hou, S. Bai, M.Z. Wang, H.M. Cheng, Adsorption and capillary of nitrogen in aggregated multi-walled carbon nanotubes, Chem. Phys. Lett. 345 (2001) 18–24.
[57] S. Furmaniak, A.P. Terzyk, P.A. Gauden, K. Lota, E. Frąckowiak, F. Béguin, P. Kowalczyk, Determination of the space between closed multiwalled carbon nanotubes by GCMC simulation of nitrogen adsorption, J. Colloid Interface Sci. 317 (2008) 442–448.
[58] K. Yang, B. Xing, Desorption of polycyclic aromatic hydrocarbons from carbon nanomaterials in water, Environ. Pollut. 145 (2007) 529–537.
[59] H.H. Cho, B.A. Smith, J.D. Wnuk, D.H. Fairbrother, W.P. Ball, Influence of surface oxides on the adsorption of naphthalene onto multiwalled carbon nanotubes, Environ. Sci. Technol. 42 (2008) 2899–2905.
[60] O. Ingolfsson, E. Illenberger, Electron attachment reactions in mixed SF_6/N_2 clusters, Chem. Phys. Lett. 241 (1995) 180–184.
[61] S. Sircar, Isosteric heat of multicomponent gas adsorption on heterogeneous adsorbents, Langmuir 7 (1991) 3065–3069.